HHS Public Access

Author manuscript

Hum Pathol. Author manuscript; available in PMC 2022 August 15.

Published in final edited form as:

Hum Pathol. 2021 August ; 114: 74–89. doi:10.1016/j.humpath.2021.05.004.

Intraductal carcinoma of the salivary gland with *NCOA4-RET*: expanding the morphologic spectrum and an algorithmic diagnostic approach☆

Adam S. Fisch[a,d,1], **Israa Laklouk**[a,d,1], **Masato Nakaguro**[a,d], **Vânia Nosé**[a,d], **Lori J. Wirth**[b,e], **Daniel G. Deschler**[c,f], **William C. Faquin**[a,c,d], **Dora Dias-Santagata**[a,d], **Peter M. Sadow**[a,c,d,*]

[a]Pathology Service, Massachusetts General Hospital, 02114 USA

[b]Department of Medicine, Massachusetts General Hospital, 02114 USA

[c]Department of Otolaryngology, Massachusetts Eye and Ear, 02114 USA

[d]Department of Pathology, Harvard Medical School, Boston, MA, 02115 USA

[e]Department of Medicine, Harvard Medical School, Boston, MA, 02115 USA

[f]Department of Otolaryngology, Harvard Medical School, Boston, MA, 02115 USA

Summary

After the publication of the 2017 World Health Organization Classification of Head and Neck Tumours, there has been increasing interest in the classification of newly categorized intraductal carcinomas. Intraductal carcinoma (IC) is an indolent tumor, typically arising in the parotid gland, with an intact myoepithelial layer and a cystic, papillary, often cribriform architecture. Early studies of IC identified a heterogeneous group of molecular alterations driving neoplasia, and recent studies have defined three primary morphological/immunohistochemical variants, subsequently linking these morphologic variants with defined molecular signatures. Although studies to date have pointed toward distinct molecular alterations after histological classification, this study used a novel approach, focusing primarily on six cases of IC with *NCOA4-RET* gene rearrangement as determined by next-generation sequencing and describing the spectrum of clinicopathologic findings within that molecularly-defined group, among them a unique association between the *NCOA4-RET* fusion and hybrid variant IC and the first case of IC arising in association with a pleomorphic adenoma. *RET*-rearranged IC show histological and immunohistochemical overlap with the more widely recognized secretory carcinoma, including low-grade morphology, a lumen-forming or microcystic growth pattern, and co-expression of S100, SOX10, and mammaglobin, findings undoubtedly leading to misdiagnosis. Typically regarded to have *ETV6-NTRK3* fusions, secretory carcinomas may alternatively arise with *RET* fusions as well. Adding our cohort of six *NCOA4-RET* fusion-positive IC compared with four cases of secretory carcinoma with *ETV6-RET* fusions and a single case of fusion-negative IC with salivary duct carcinoma-like genetics, we propose a diagnostic algorithm that integrates

☆Competing interests: The authors declare no relevant conflict of interests.

*Corresponding author. Massachusetts General Hospital, Pathology Service, Department of Pathology, WRN219, 55 Fruit Street, Boston, MA 02114, USA. psadow@mgh.harvard.edu (P.M. Sadow).

[1]These authors contributed equally to this article.

histological elements, including atypia and invasiveness, and the likelihood of specific molecular alterations to increase diagnostic accuracy in what can be a very subtle diagnosis with important clinical implications.

Keywords

Intraductal carcinoma; Salivary gland carcinoma; *NCOA4-RET*; *ETV6-RET*; Secretory carcinoma

1. Introduction

Since the 2017 World Health Organization Classification of Head and Neck Tumours [1], the characterization of the newly designated “intraductal carcinoma” in terms of its molecular and histomorphological features has garnered increased interest. Intraductal carcinoma (IC), originally described by Chen et al. in 1983 [2], has been formerly called low-grade cribriform cystadenocarcinoma and low-grade salivary duct carcinoma (SDC) [3–5]. Clinically, IC almost exclusively arises in the parotid and follows an indolent clinical course after complete resection [3,6]. Histologically, IC typically has micropapillary and cribriform architecture arising within ducts that are surrounded by an intact layer of myoepithelial cells, highlighted by immunohistochemistry, except for cases with an invasive component. There is often associated hemorrhage, foamy macrophages, and eosinophilic luminal secretions, resembling atypical ductal hyperplasia and ductal carcinoma in situ of the breast. Despite its relative rarity, three distinct morphological variants have been described in previous studies: intercalated duct, apocrine, and hybrid intercalated and apocrine [2–4,7,8].

Histologically, intercalated duct IC is comprised of bland, small to medium tumor cells with ovoid nuclei containing fine chromatin, occasional distinct nucleoli, and amphophilic cytoplasm [7–9]. In contrast, apocrine IC cells have intermediate- to high-grade nuclei with prominent nucleoli and abundant eosinophilic cytoplasm with apical snouts and luminal cytoplasmic decapitations [7]. In addition to morphologic features, these two main phenotypes can largely be distinguished by their mutually exclusive immunohistochemical profiles, namely, positive staining for S100, SOX10, and mammaglobin in intercalated duct IC, and nuclear positive androgen receptor (AR) in apocrine IC. More recently, studies have shown that apocrine IC with low-grade histology has similar immunohistochemical and molecular features as its higher grade apocrine counterpart [10] and that the molecular findings in IC with partial or pure oncocytic morphology include alterations in *RET* and *BRAF* [11].

Initial investigations into the molecular features of IC by Weinreb et al. [7] established a clear distinction in genetic alterations between the intercalated duct-type intraductal tumors with *RET* translocations and apocrine-type intraductal tumors with SDC-like genetics, including single-nucleotide variants (SNVs) in *PIK3CA* and *HRAS*, as well as *HER2* amplification, the latter with treatment implications. Further molecular studies in expanded cohorts by Skálová et al. [8,9] correlated histopathological features, including morphology and immunohistochemistry, with molecular alterations. In addition to reaffirming the

SDC-like molecular features of pure apocrine IC, hybrid lesions were found to have molecular overlap with intercalated duct IC by harboring *RET* translocations. Mirroring the imperfect histological overlap of intercalated duct and hybrid IC, however, were the subtly divergent fusion partners with *RET*; *NCOA4-RET* is seen in approximately half of the pure intercalated duct tumors, and the far less common *TRIM27*-RET fusion has only been seen in a subset of hybrid IC.

As with pathological characterization of most newly recognized tumors, the molecular features are described as a diagnostic correlate of the histological diagnosis, and despite the rarity of an IC diagnosis, the more the entity is recognized and characterized, the morphologic and genetic correlations grow clearer and modify initial descriptions of discrete entities. In this study, we present six cases of IC with *NCOA4-RET* fusion to broaden the morphological spectrum and clinical context of *RET*-rearranged IC as a function of this molecular signature.

Molecular diagnostics is rapidly changing the precise classification of salivary carcinomas. Secretory carcinoma (SC), first described just over 10 years ago [12], provided a genetic fusion driver, *ETV6-NTRK3*, for a distinct set of carcinomas thought to be a more aggressive subtype of acinic cell carcinoma (ACC) [13]. Over the next decade, as this tumor became more commonly recognized morphologically, the distinction between tumor types, facilitated by subtle morphologic differences and differences in immunohistochemical expression (S100 in SC and DOG1 in ACC) [14], seemingly clarified the ACC versus SC issue, especially with the distinct fusion protein of SC. Salivary gland tumors in which the intercalated duct variant of IC is in the differential diagnosis must also include SC. Morphologically, SC is a low-grade salivary gland carcinoma with overlapping morphological (ie, formation of small cysts/ spaces with eosinophilic luminal secretions) and immunohistochemical (ie, S100, SOX10, and mammaglobin expression) features [15,16] with intercalated duct-type IC. Historically, the characteristic gene fusion of *ETV6-NTRK3*, which is also seen in SC of the breast, could help distinguish SC from other entities in the differential diagnosis; however, recent discoveries of SC harboring alternative fusions, including those that incorporate *RET* [15,16], have given additional nuance to salivary gland diagnostics. By comparing the features of six cases of *RET*-rearranged IC with four cases of SC harboring *ETV6-RET* fusions and a single case of IC with an SDC-like molecular signature, we will highlight novel pathologic features in IC, including a newly described histological–molecular association in hybrid variant IC, the first case of IC arising in contiguity with a pleomorphic adenoma (PA), and a Warthin-like, focally oncocytic IC arising in an intraparotid lymph node. These features will be integrated with previously published data to generate a diagnostic algorithm to differentiate IC variants and SC.

2. Material and methods

2.1. Case identification

Pathology archives were reviewed for patients with *RET*-rearranged salivary carcinomas treated at affiliated academic tertiary referral centers (Massachusetts Eye and Ear and Massachusetts General Hospital [MGH], Boston, MA) from March 2014 to January 2021.

The study was approved by the Mass General Brigham (MGB) Institutional Review Board (2015P001749, P.M.S.).

The MGH molecular database was reviewed for cases of primary salivary gland tumors subjected to targeted gene rearrangement next-generation sequencing (NGS). The diagnostic hematoxylin and eosin (H&E)-stained slides along with ancillary studies of the *RET*-rearranged salivary gland carcinomas were retrieved from the surgical pathology archives of MGH. An additional case of IC, almost entirely surrounded by an intact myoepithelial layer and identified to have an SDC-like genetic signature, was incorporated into the study for further histologic comparison with *RET*-translocated salivary gland carcinomas. The selected cases were reviewed, and final diagnoses were made based on histological, immunohistochemical, and molecular studies by four head and neck pathologists (A.S.F., I.L., M.N., and P.M.S.). The diagnostic criteria were based on studies from the 2017 edition of the World Health Organization's Classification of Head and Neck Tumours [1].

2.2. Demographic data and clinical course

The demographics, treatment, and follow-up details were obtained from the MGB electronic medical records. Demographic data included age at initial diagnosis, sex, anatomic site and tumor size, smoking status, and prior radiation exposure. Diagnostic characteristics of each case included the duration of symptoms before diagnosis and whether they included pain, pathologic TNM classification, and stage/prognostic group according to the current American Joint Committee on Cancer classification (8th edition) [17]. Treatment and follow-up data included therapeutic modality (resection, lymph node dissection, and adjuvant therapy), follow-up time since treatment, and long-term outcome (no evidence of disease, recurrent disease, metastatic disease, or disease-related death).

2.3. Histological evaluation

Completely resected lesions in the study were assessed for adverse histological features as defined by the National Comprehensive Cancer Network Guideline Version 1.2021 for major salivary gland tumors [18]. These included intermediate or high-grade histomorphology, close (≤1 mm) or positive margins, neural or perineural invasion (PNI), lymph node metastases, lymphatic or vascular invasion (LVI), or pT3/pT4 tumors [18]. Additional histopathologic features were evaluated in each case, including IC variant type, presence and degree of an invasive tumor component (abluminal myoepithelial cell layer focally lost in minimally invasive and completely lost in broadly invasive), dominant tumor growth pattern (cystic, nodular, or infiltrative), stromal qualities (sclerotic or lymphoid), and extraglandular extension (EGE).

2.4. Immunohistochemistry

Immunohistochemical studies were performed using 4- to 5-μm-thick, formalin-fixed paraffin-embedded (FFPE) sections of selected blocks for 11 patients diagnosed with *RET*-rearranged salivary gland carcinomas in a Bond 3 automated immunostainer (Leica Microsystems, Bannockburn, IL) and primary antibodies directed against S100 protein (polyclonal and prediluted; Ventana, Oro Valley, AZ), mammaglobin (clone 304-1A5; dilution 1:250; Dako, Carpinteria, CA), p63 (clone 4A4; prediluted; Biocare), SOX10

(Clone BC34; Cat#ACI3099C 1:100; Biocare), CD117 (clone EP10, prediluted, BioSB), DOG1 (clone K9, ready to use, Leica Cat# PA0219), mucicarmine (cat#860-011, ready to use), and AR (clone BSB-4; prediluted, BioSB). Appropriate positive and negative controls were included. The immunohistochemical slides were reviewed by four MGH head and neck pathologists (A.S.F., I.L., M.N., and P.M.S.).

2.5. Molecular analysis

NGS was performed as part of routine clinical diagnostics using the laboratory's "Solid Fusion Assay." Total nucleic acid was extracted from FFPE tissue, with libraries subsequently prepared for sequencing using an anchored multiplex PCR platform, as described previously 19 (Hu B et al.) which covered the following genes (exons): *ALK* (19–22, intron 19), *BRAF* (7–12, 15), *EGFR* (2–7 exon skipping/VIII variant, 7–9, 16, 20, 24, 25), *EWSR1* (4–14), *FGFR2* (2, 8–10, 17), *MAML2* (2,3), *MET* (exon 14 skipping), *NRG1* (1–3, 6), *NUTM1* (3), *RET* (8–13), *ROS1* (31–37), *AKT3* (1–3), *ARHGAP26* (2, 10–12), *AXL* (19, 20), *BRAF* (7–12, 15), *BRD3* (9–12), *BRD4* (10, 11), *ERG* (2–11), *ESR1* (3–6), *ETV1* (3–13), *ETV4* (2, 4–10), *ETV5* (2, 3, 7–9), *ETV6* (1–7), *FGFR1* (2, 8–10, 17), *FGFR3* (8–10, 17, intron 17), *FGR* (2), *INSR* (12–22), *JAZF1* (2–4), *MAML2* (2, 3), *MAST1* (7–9, 18–21), *MAST2* (2, 3, 5, 6), *MET* (13, 15), *MSMB* (2–4), *MUSK* (7–9, 11–14), *MYB* (7–9, 11–16), *NOTCH1* (2, 4, 26–31, internal exon 3–27 deletion), *NOTCH2* (5–7, 26–28), *NRG1* (1–3, 6), *NTRK1* (8, 10–13), *NTRK2* (11–17), *NTRK3* (13–16), *NUMBL* (3), *PDGFRA* (7, exon 8 deletion, 10–14), *PDGFRB* (8–14), *PIK3CA* (2), *PKN1* (10–13), *PPARG* (1–3), *PRKCA* (4–6), *PRKCB* (3), *RAF1* (4–7, 9–12), *RELA* (3, 4), *RSPO2* (1, 2), *RSPO3* (2), *TERT* (2), *TFE3* (2–8), *TFEB* (1, 2), *THADA* (28), and *TMPRSS2* (1–6). Illumina MiSeq 2 × 147 base paired-end reads were mapped to the hg19 human reference genome using BWA-MEM (20) Palicelli. The target genes of this panel were selected for diagnosis, prognosis, and identification of potential therapeutic targets. The assay was performed in a Clinical Laboratory Improvement Amendments (CLIA)-accredited laboratory at MGH, analyzed by a clinically validated pipeline, and results were reviewed and interpreted by molecular pathologists (A.S.F. and D.D.S.). Confirmatory fluorescence in situ hybridization (FISH) was performed in a subset of cases using break-apart probes for the *RET* gene as well as *HER2* probes for copy number assessment.

3. Results

3.1. Molecular characteristics

A total of 463 tumors of the head and neck were subjected to NGS to identify targeted gene rearrangements at MGH pathology in 2016–2021. *RET* rearrangements were identified in 10 salivary gland tumors, including *NCOA4-RET* in six cases of IC and *ETV6-RET* in four cases of SC (Fig. 1) [19]. No other *RET* fusion partners were identified in this anatomic location. In IC, the fusion breakpoints in *NCOA4* were exons 7 and 8, whereas the *RET* breakpoint was exon 12. No additional or ancillary molecular testing was performed on these samples. In SC, the *ETV6* genetic breakpoint was consistently exon 6, whereas the *RET* genetic breakpoint was variable, including exon 10 and exon 12. *RET* translocation was confirmed by break-apart FISH in cases 9 and 11. An additional case of IC with apocrine morphology showed no fusion, was positive for SNVs in *HRAS* c.181C>A

(p.Q16K) and *PIK3CA* c.1624G>A (p.E542K), and showed no amplification of *HER2* with NGS or FISH.

3.2. Histomorphological and immunohistochemical characteristics

Histomorphological and immunohistochemical characteristics of the 10 RET-rearranged salivary gland carcinomas and one apocrine IC are summarized in Table 1. In total, all 10 evaluable cases (100%), including two recurrent tumors, had at least one adverse histological feature at the time of diagnosis, including four cases with close margins, four cases with intermediate- or high-grade histomorphology, two cases with positive margins, two cases with LVI, and two cases with neural or PNI (intraoperatively discovered in Cases 3 and 5 and histologically identified in Case 5). No patients presented with lymph node metastases.

3.2.1. Intraductal carcinoma with *NCOA4-RET* fusion—Among the six cases of IC harboring an *NCOA4-RET* fusion, three were initially diagnosed as SC, two were diagnosed as IC, and one was diagnosed as carcinoma ex-pleomorphic adenoma (CEPA). After rereview of these cases in the context of molecular data plus additional immunohistochemistry, all were classified as IC.

Of these six tumors, two cases showed pure intercalated duct-type morphology, two tumors had focal oncocytic morphology, and two specimens were classified as a hybrid variant of IC with combined intercalated duct and apocrine components. Intercalated duct morphology included papillary-cystic or nodular architecture containing solid or cribriform formations (Fig. 2A) of tumor cells with low-grade cytomorphology and round-to-ovoid nuclei containing fine chromatin as well as moderate-to-abundant eosinophilic cytoplasm (Fig. 2B). In two tumors, focal oncocytic cells demonstrated large cellular size with relatively round nuclei and distinct nucleoli surrounded by abundant eosinophilic, granular cytoplasm with distinct cellular borders. One of the focally oncocytic cases (Case 2) showed a broadly infiltrative tumor front with pushing invasive growth. Immunohistochemically, all areas with intercalated duct or oncocytic morphology showed diffuse and strong expression of S100 (Fig. 2C), SOX10 (Fig. 2D), and mammaglobin (Fig. 2E), with negative staining for AR (Fig. 2E inset), and an intact, p63-positive myoepithelial cell layer (Fig. 2F) with the exception of Case 2 (Fig. 3), where the invasive component that lacked the latter (Fig. 3F). One patient presented with a pure intercalated duct variant IC (Case 5) arising in contiguity with a PA, with PLAG1 immunohistochemistry showing nuclear reactivity in the PA (Fig. 2A).

The two remaining cases showed hybrid morphology. One case (Case 4; Fig. 4A and B) had diminutive ductal formation within the sclerotic stroma for which apocrine-type histomorphology was difficult to appreciate (Fig. 4C), but in which nuclear positivity for AR (Fig. 4D), loss of S100 (Fig. 4E), and decreased staining proportion and intensity for SOX10 were all apparent. The myoepithelial cell layer was intact around these ducts, as demonstrated by CK5/6 staining (Fig. 4F) and p63. This case also showed a heterogeneous histomorphology, with a distinct population of intermediate-grade tumor cells comprising more than half of the lesion and demonstrating larger, wider nuclei with smooth nuclear contours, fine vesicular chromatin, one to two distinct nucleoli, and amphophilic cytoplasm

(Fig. 4B). The intermediate-grade cells showed no distinct cellular borders, displayed a more overlapped, jumbled appearance than the lower grade intercalated duct tumor counterparts, and showed cytoplasmic staining for AR (not shown). The final case with hybrid morphology (Case 6) was composed of an even distribution of intercalated duct and low-grade apocrine tumor cells (Fig. 5A), the latter demonstrating cystic dilation with one layer of low-grade cuboidal to columnar cells containing small ovoid nuclei, fine chromatin, and brightly eosinophilic apical cytoplasm; the vast majority of these cells also had apical snouts and luminal decapitations (Fig. 5B). Immunohistochemically, S100 (Fig. 5C) and SOX10 were positive in the intercalated duct component of the tumor, whereas apocrine areas were negative for these markers and demonstrated more intense and abundant membranous staining with HER2 (Fig. 5D); both components showed diffuse staining for mammaglobin (Fig. 5E). One large intraductal papillary formation (Fig. 5F) of tumor cells showed intermingling of intercalated duct and columnar cells with apical projections most resembling apocrine morphology (Fig. 5G), with the respective immunophenotypes in each portion of the proliferation (Fig. 5G inset), and interspersed mucin-containing cells. AR was negative throughout the tumor, and all tumor foci were bound by p63- and calponin-positive myoepithelial cells (not shown).

All six *RET*-rearranged IC showed similar cytologic features at the luminal surface of each architectural formation, specifically lateral or perpendicular cytoplasmic elongation of lumen-facing cells in a wrapping, “umbrella”-like formation, and cytoplasmic vacuolization showing an abundant, more intensely eosinophilic cytoplasm (Fig. 6). Evaluation of the stroma in these tumors revealed five cases with a lymphoid component, including four with tumor-associated lymphoid proliferation (TALP) and one arising within an intraparotid lymph node (Case 2). All but Cases 2 and 3 had an at least partially sclerotic stroma. Additional immunohistochemical markers and stains included CD117 (N = 5), mucicarmine (N = 4), and DOG1 (N = 3). CD117 showed variable reactivity, with focally positive cells (4/5, 80%) most intensely staining at the abluminal border and decreasing in intensity inward as a gradient in three cases, and a reverse gradient with most intense staining at the luminal border in one case. Mucicarmine highlighted the secretions within cribriform spaces and the cytoplasm of mucin-containing cells, such as in Case 6. DOG1 also showed focal reactivity, consistently staining the abluminal layers of tumor cells most intensely in the three cases in which it was tested (not shown).

3.2.2. Intraductal carcinoma with an SDC-like molecular signature—One tumor was identified as an apocrine IC by a combined morphological-molecular approach. Histological evaluation showed multiple dilated ductal proliferations with a so-called “filigreed” papillary architecture containing “Roman bridge” formations and extensive tufting. The tumor cells’ cytomorphology showed intermediate to high-grade nuclear features, large nuclei with irregular membranes, condensed chromatin, and abundant apically oriented eosinophilic, sometimes glassy, cytoplasm (Fig. 5H). Multiple invasive foci were appreciated with an associated fibrotic stromal reaction and hyalinization (Fig. 5H inset). Molecular testing identified two SNVs, *HRAS* p.Q16K and *PIK3CA* p.E542K, no fusions on NGS, and no amplification of *HER2* on NGS or FISH.

3.2.3. Secretory carcinoma with *ETV6-RET* fusion—

Among the four cases of SC identified to have *ETV6-RET* fusions, two cases were originally diagnosed as SC, one case was called CEPA, and one tumor had a remote excision, and the slides and report from the primary resection were not available for review. After the identification of *ETV6-RET* fusions, as well as recent publications describing salivary gland SC harboring this specific molecular alteration, the cases with original non-SC diagnoses were rereviewed and reclassified as SC.

Of the three SC cases with slides available for review, two were from tumor recurrences (Cases 9 and 10), and one primary tumor resection (Case 8). All three cases showed similar morphological features, specifically broadly invasive lobules separated by fibrous septa containing tumor nodules with cribriform architecture containing eosinophilic luminal secretions. Neoplastic cells had abundant eosinophilic cytoplasm and uniform small- to medium-sized ovoid nuclei with delicate-to-vesicular fine chromatin and occasional small nucleoli (Fig. 6B) and abundant eosinophilic or vacuolated cytoplasm with dispersed microcyst formation. Two cases (Cases 9 and 10) also showed a distinct infiltrative component as well as a transition to intermediate atypical morphology. Lymphatic invasion was identified in one case (Case 8), and EGE was observed in two patients' tumors (Case 8 and Case 10). Immunohistochemistry showed diffuse and strong reactivity for S100 and SOX10, with S100 also positive in Case 11 by report. Mammaglobin was diffusely positive in three of the four cases tested, and its reactivity in only rare cells of Case 10 led to the consideration of a diagnosis of adenocarcinoma, NOS. AR was negative in all cases tested. The presence of p63-positive myoepithelial rimming was only focally observed in one case (Case 9), suggesting an intraductal component, and was otherwise absent from all cases, consistent with broad invasion.

3.3. Clinical characteristics and treatment outcome

The main demographic and clinical characteristics of the 11 patients at the time of diagnosis are summarized in Table 1. Overall, there were seven females and four males (male:female 1:1.75), with a mean age of 55.6 years (range: 44–88 years). The mean tumor size was 2.4 cm (range: 1.4–3.8 cm). Ten cases arose in the parotid gland, whereas one developed in the submandibular gland. None of the patients had any prior exposure to radiation. On average, symptoms lasted 14.5 months (range: 1–48 months) from onset to diagnosis, and only one patient presented with pain. From the patients with evaluable primary tumors and associated clinical records, a total of five patients were determined to have Stage II disease (one patient's unresected tumor was staged clinically), three patients were diagnosed with Stage I disease, and one patient was clinically determined to have Stage IVc disease. Nine patients underwent complete resection of their tumors through a parotidectomy approach. Five of these patients received postoperative radiation therapy for risk factors described on final pathology (PNI, positive margins, LVI, and EGE). One patient, who at exploration had facial nerve involvement, underwent biopsy and full course external beam radiation therapy. Two patients had lymph node dissections at the time of primary resection (Cases 8 and 10). Clinical follow-up averaged 77.5 months (range 1–337 months), and 10 patients are currently alive with no evidence of disease, whereas two patients with SC have experienced multiple recurrences (Cases 9 and 10), and one patient with SC died of disease (Case 11).

4. Discussion

Over the past 15 years, significant studies have led to the recognition of a distinct salivary gland neoplasm that is predominantly noninvasive, with unique morphological features and predictable molecular alterations, culminating in its inclusion and classification as IC in the 2017 WHO Blue Book [1]. Since this classification, there has been increased focus on IC, with published series highlighting its features for pathologic diagnostic recognition [7–10,20–23]. At our institution, increased awareness of IC has led to a higher frequency of identification in our patient cohort over the last few years, and as noted in our cohort, some in retrospective review.

With a relative paucity of IC characterized in the literature when compared with other, longer-recognized salivary gland carcinomas, this cohort of IC cases are intended to broaden the field's appreciation for the clinicopathologic features of IC and its spectrum of morphologies and diagnostic overlaps. Through a molecular-first approach, focusing on the tumor variant most frequently described in IC and with the highest molecular-to-histological fidelity, the *NCOA4-RET* fusions in IC served as the baseline on which novel clinical, histological, and immunohistochemical observations can be made.

Among the three main variants of IC, *NCOA4-RET* is thought to be present in approximately half of cases [7] with intercalated duct-type morphology, and, so far, has not been observed in cases lacking at least a component of intercalated duct features [9]. Apocrine variants of IC resemble SDC in morphology, immunohistochemistry, and molecular findings [7], with the apocrine IC-SDC distinction relying on relative proportion of intraductal and invasive tumor. Hybrid tumors show both morphologies with respective immunohistochemical profiles and, in the few tumors tested, contain molecular profiles resembling pure intercalated duct variant over apocrine variants, with *TRIM27*-RET fusions [9]. Oncocytic IC has been shown to have an identical immunohistochemical profile with intercalated duct IC, and molecular analysis has similarly shown *RET* translocations, with fusion partners *NCOA4* and *TRIM33*, as well as mutually exclusive cases with *BRAF* p.V600E variants [11,23].

Here, we presented two cases of hybrid IC with *NCOA4-RET* fusions. In one case, the apocrine component is focal, represented by a group of small, low-grade ductal profiles embedded in sclerotic stroma that show positive reactivity to AR and loss of staining for S100, while maintaining an intact myoepithelial layer on p63 and CK5/6 immunohistochemistry. Although prior cases of hybrid IC have shown low-grade cytomorphology in both components [8], this case showed a distinct transition to intermediate cytomorphology in the intercalated duct component, imparting a unique appearance from all the other IC cases with intercalated duct morphology. The overlapping cells and amphophilic nuclei with small nucleoli are similar to those in Fig. 1F from Rooper et al.'s series of ICs arising in intraparotid lymph nodes [21]. The other case of hybrid IC bearing an *NCOA4-RET* fusion showed a far greater amount of low-grade apocrine ducts with distinct, evident apocrine features, including apical snouts and luminal decapitations. Interestingly, none of the apocrine areas in Case 6 were reactive to AR antibody, but other immunohistochemical markers were noticeably different from intercalated duct areas,

including loss of S100 and SOX10, and more prominent staining for HER2. Although hybrid variants are less common in the literature, the subset of cases tested by NGS that yielded positive findings was found to have only *TRIM27-RET* fusions [8,9], and the cases presented in our study are the first examples of hybrid variant IC with definitive *NCOA4-RET* fusions identified by NGS. Although it was unexpected, the lack of AR staining in Case 6 is not the first example of discordant morphological and AR findings in the context of this group of lesions. In Wang et al. [24], two cases of SDC with *NCOA4-RET* fusions are described, but the image portraying AR staining shows only partial staining of tumor cells, which raises the question of whether these cases were in fact IC with hybrid morphology, as others have also mentioned [21]. This phenomenon of aberrant AR staining, along with the detection of the characteristic intercalated duct gene fusion *NCOA4-RET* and the often low-grade appearance of apocrine components in hybrid tumors, supports the notion that these apocrine cells are molecularly distinct from those of pure apocrine IC, and the formation of apocrine cells in hybrid tumors is possibly a late event without a distinct molecular driver, perhaps as a reactive change or transdifferentiation of intercalated duct tumor cells.

Two of the intercalated duct variant IC cases also had focal oncocytic change, one arising in an apparent intraparotid lymph node, which, in contrast to the multiple cases in our cohort with TALP, had an evident capsule and subcapsular sinus, consistent with prior descriptions [21,25]. As previously described by Bishop et al., molecular analysis of oncocytic IC has shown significant overlap with intercalated duct, both often possessing a *RET*-rearranged driver alteration, with a subset of oncocytic IC harboring *BRAF* p.V600E variants [11]. Although others have described IC arising in an intraparotid lymph node [5,21,26], this is the first time oncocytic cells have been identified in that setting; the oncocytic cells lacked the typical two-layered appearance, but a larger proportion of oncocytic cells embedded in lymphoid stroma could bear a histologic resemblance to a Warthin tumor, a possible diagnostic pitfall on cytology if sampled during fine needle aspiration. The latter case, Case 2, was broadly invasive, with tumor pushing into the surrounding lymphoid stroma toward the capsule with complete loss of myoepithelial markers in the area, adding another rare case of widely invasive intercalated duct IC to the literature [7,9].

Furthermore, in our cohort, there were two cases with facial nerve involvement appreciated intraoperatively (clinically), with one of the cases also demonstrating PNI histologically. It was noteworthy that these two patients presented with a long-standing history of a parotid mass for >60 months, and this may suggest that this invasive morphology may be a result of progression in this typically indolent tumor's clinical course.

Interestingly, Case 5 arose in the parotid gland, in contiguity with a PA, raising the possibility of a yet-described intraductal carcinoma ex-pleomorphic adenoma (ICEPA). A subset of PAs harbor translocations involving *PLAG1* and *HMGA2* [27–29], which can be assessed by immunohistochemistry or molecular testing. PLAG1 immunohistochemistry in Case 5 showed positive nuclear reactivity in the PA component and no reactivity in the IC component. Although multiple studies have shown the presence of *PLAG1* and *HMGA2* genetic alterations in cases of CEPA [24,30–34], few have reported the results of immunohistochemical or molecular testing performed on distinct microdissected

tumor components, and there is a dearth of explicit data regarding the concordance of signal between PA and the carcinomatous component of CEPA [32,33]. Among reports that provided this level of information, discordant results between the PA and malignant components of CEPA have been observed as *HMGA2* alterations detected in the carcinomatous component and not the PA component [33], as well as loss of PLAG1 immunohistochemical reactivity in the carcinomatous component despite retained positive staining in the PA component [32]. Taking into account the histological proximity between the two tumor components present as well as the aggressive clinical nature of the tumor in Case 5, specifically the gross involvement of the facial nerve intraoperatively, this unique tumor does not align with the typical clinical course of IC. If indeed it does represent ICEPA, it is interesting to note that the nodular structures of the IC component lacked infiltration or invasion, confirmed by retention of p63-positive myoepithelial cells, which would lend credence to the findings by Bishop et al. that myoepithelial cells are also a neoplastic component of these tumors [35].

The histological, immunohistochemical, and molecular findings in SC have been emerging for just over a decade and now include SC with *ETV6-RET* fusions [15,16,36–38]. As the awareness of different morphological variants and associated findings on ancillary testing (eg, diffuse positivity for S100, SOX10, and mammaglobin) in IC grows, there is an emerging pitfall in the differentiation between intercalated duct IC and SC, two low-grade malignancies with seemingly subtle morphologic/architectural differences. Histologically, both are composed of cribriform or microcystic growth of bland neoplastic cells. Skalova et al. described three primary morphological patterns of SC in a cohort of tumors with *ETV6-RET* fusions. These patterns included a multicystic growth pattern with mural nodules, a solid and microcystic multilobular architecture with fibrous septae, and a fibrosclerotic stroma with isolated tumor cells in small islands and trabeculae [14] that bear a strong resemblance to cystic intercalated duct tumors, nodular intercalated duct tumors, and apocrine tumors in our IC cohort, respectively. All cases of SC in our cohort resembled the second pattern proposed by Skalova et al., and its most similar pattern of growth in IC, specifically nodular growth, was the most frequent architecture seen in our cases. Beyond histology, even some molecular testing modalities for *RET* rearrangements are not a guaranteed method to distinguish these two entities; the presence of newly identified morphological features in our IC cohort, including luminal cells with cytoplasmic vacuolation, is often seen in SC [15] and can further exacerbate attempts to reach a definitive diagnosis in this differential.

To provide guidance in differentiating these two very similar tumors, we propose a diagnostic algorithm integrating morphological findings, immunohistochemical reactivity, and molecular alterations (Fig. 7). On initial histological review, a well-circumscribed cystic or nodular salivary gland tumor, later confirmed to have an intact myoepithelial layer by immunohistochemistry, should prompt an initial histomorphological assessment of cell type and grade of atypia. High-grade apocrine morphology comprises the apocrine variant of IC and can be confirmed by immunohistochemistry and molecular testing; any other high-grade morphology should be evaluated as a different invasive entity with a predominantly intraductal component on presentation. Among low-grade intraductal tumors with a nonspecific ductal appearance, the cells will have variable amounts of cytoplasm,

secreted material in luminal spaces, and typically an S100-, SOX10-, and mammaglobin-positive immunohistochemical profile. Although the presence of p63-positive myoepithelial rimming is a helpful clue in the differential diagnosis [6,7], the differentiation between SC with intraductal growth and intercalated duct IC with invasive growth can be confounding [7–10]. Oncocytic morphology in IC has been increasingly reported in recent studies, and identification of a *RET* fusion, including *TRIM33*-RET and *NCOA4-RET*, or a BRAF p.V600E variant can further support the diagnosis of IC. The presence of at least some component of apocrine morphology is helpful in suggesting the hybrid variant of IC because SC does not have a known apocrine component and can be confirmed by the identification of an *NCOA4-RET* or *TRIM27*-RET fusion; the former fusion's presence in hybrid IC is based on the findings of this study, and the latter fusion can also be identified on break-apart FISH for *RET*.

In tumors of pure ductal morphology, the final diagnosis requires molecular insight. In the laboratory setting where FISH is routinely performed over broad NGS panels, *ETV6* break-apart *FISH* can be helpful, where a positive result confers an extremely high likelihood that the tumor is an SC with an intraductal component. Although non-*ETV6* fusions have been identified in SC [39–41], its well-documented recurrent *ETV6-NTRK3* and *ETV6-RET* fusions mean a negative *ETV6* FISH result should favor IC. *RET* lies very close to *NCOA4* on chromosome 10q11.2, leading to an intrachromosomal fusion that is difficult to appreciate by break-apart FISH for *RET*, so it is not advised for the identification of pure intercalated duct IC.

If a laboratory has access to the routine use of a broad NGS panel to detect fusions involving *RET*, *ETV6*, or *NTRK3*, a fusion involving *ETV6*, whether with *RET* or *NTRK3*, is indicative of an SC with an intraductal component. The presence of an *NCOA4-RET* fusion is diagnostic of an intercalated duct IC, and aside from case reports of specific fusions in IC (*STRN-ALK*) [21] and SC (*VIM-RET*), identification of other fusions would be novel and likely favor IC over SC in the context of a tumor with predominantly intraductal and indolent clinicopathologic features. A result where no fusions are identified favors a fusion-negative intercalated duct IC because *NCOA4-RET* fusions were found in approximately half of the intercalated duct cases tested previously, and SC is generally defined by its fusion.

Determining the appropriate diagnosis extends beyond prognostic implications, where intercalated duct IC is indolent and effectively cured by complete resection and SC may be more variable in its clinical course; molecular confirmation of both fusion partners by NGS is essential whenever targeted therapies are considered. Although FISH assays are useful surrogates for NGS in expediting the turnaround time and reducing costs, one case in our series demonstrates the limitations of this approach; in Case 11, the patient's sample was tested initially with *ETV6* FISH, yielding a positive result with a presumptive *NTRK3* fusion partner. Had the patient's sample not been tested with confirmatory NGS, identifying an *ETV6-RET* fusion, the patient might have received NTRK-targeted therapy rather than the appropriately received RET-targeted alectinib. Differentiation of intercalated duct IC from SC, most commonly harboring *NCOA4-RET* and *ETV6-NTRK3* drivers, respectively,

as well as either entity from SC with an *ETV6-RET* fusion, is essential for selecting appropriate management in the setting of advanced disease.

This study presented cases that shared a common driver alteration, namely, *RET* translocations. *RET*-driven malignancies have been described in tumors from various sites, most prominently the lung and thyroid [42–44], with more recent associations described in tumors of the breast and pancreas [45–48]. Driver alterations in *RET* typically activate the protein through hotspot SNVs or gene fusions. The treatment of *RET*-altered tumors has gone through a significant evolution in terms of mechanism of action and specificity. Cytotoxic agents have been recommended for metastatic *RET*-driven malignancies in the past [49], and in the last decade, the use of targeted therapy against the RET protein through multikinase inhibition with cabozantinib [50] and vandetanib [51] has had success but has had unfavorable adverse event profiles, often due to VEGFR2-inhibiting potential. More recently, *RET*-specific targeted inhibitors, specifically selpercatinib and pralsetinib, have had a transformative effect on *RET*-altered lung and thyroid cancer, with objective response rates ranging from 56% to 63% [52–55]. With novel therapies showing efficacy and high specificity for this molecular signature, patients with salivary gland carcinomas harboring these fusion-driven kinases, especially those with persistent, recurrent, or advanced disease, would likely benefit from the therapeutic developments against this driver that have been successful in other malignancies. Therefore, it is particularly important for these entities to be recognized pathologically, especially given architectural and histological overlap, and the data presented herein suggest this algorithm-based diagnostic approach should reap the most benefit for pathologic diagnosis and, most importantly, directed patient therapy.

Funding/Support:

NIH NCI 1P01CA240239-01 (P.M.S., W.C.F., and L.J.W.).

References

[1]. El-Naggar A, Chan J, Grandis J, Takata T, Slootweg P. WHO Classification of Head and Neck Tumours. 4th ed. IARC Press; 2017.

[2]. Chen KTK. Intraductal carcinoma of the minor salivary gland. J Laryngol Otol 1983;97:189–92. 10.1017/S002221510009397X. [PubMed: 6298331]

[3]. Delgado R, Klimstra D, Albores-Saavedra J. Low grade salivary duct carcinoma. A distinctive variant with a low grade histology and a predominant intraductal growth pattern. Cancer 1996;78:958–67. 10.1002/(SICI)1097-0142(19960901)78:5<958::AID-CNCR4>3.0.CO;2-8. [PubMed: 8780532]

[4]. Nakatsuka S, Harada H, Fujiyama H, Takeda K, Kitamura K, Kimura H, et al. An invasive adenocarcinoma of the accessory parotid gland: a rare example developing from a low-grade cribriform cystadenocarcinoma? Diagn Pathol 2011;6:122. 10.1186/1746-1596-6-122. [PubMed: 22151879]

[5]. Weinreb I Intraductal carcinoma of salivary gland (so-called low-grade cribriform cystadenocarcinoma) arising in an intraparotid lymph node. Head Neck Pathol 2011;5:321–5. 10.1007/s12105-011-0256-0. [PubMed: 21442195]

[6]. Brandwein-Gensler M, Hille J, Wang BY, Urken M, Gordon R, Wang LJ, et al. Low-grade salivary duct carcinoma: description of 16 cases. Am J Surg Pathol 2004;28:1040–4. 10.1097/01.pas.0000128662.66321.be. [PubMed: 15252310]

[7]. Weinreb I, Bishop JA, Chiosea SI, Seethala RR, Perez-Ordonez B, Zhang L, et al. Recurrent RET gene rearrangements in intraductal carcinomas of salivary gland. Am J Surg Pathol 2018;42:442–52. 10.1097/PAS.0000000000000952. [PubMed: 29443014]

[8]. Skálová A, Vanecek T, Uro-Coste E, Bishop JA, Weinreb I, Thompson LDR, et al. Molecular profiling of salivary gland intraductal carcinoma revealed a subset of tumors harboring NCOA4-RET and novel TRIM27-RET fusions: a report of 17 cases. Am J Surg Pathol 2018;42:1445–55. 10.1097/PAS.0000000000001133. [PubMed: 30045065]

[9]. Skálová A, Ptáková N, Santana T, Agaimy A, Ihrler S, Uro-Coste E, et al. NCOA4-RET and TRIM27-RET are characteristic gene fusions in salivary intraductal carcinoma, including invasive and metastatic tumors: is “intraductal” correct? Am J Surg Pathol 2019;43: 1303–13. 10.1097/PAS.0000000000001301. [PubMed: 31162284]

[10]. Bishop JA, Gagan J, Krane JF, Jo VY. Low-grade apocrine intraductal carcinoma: expanding the morphologic and molecular spectrum of an enigmatic salivary gland tumor. Head Neck Pathol 2020;14:869–75. 10.1007/s12105-020-01128-0. [PubMed: 31989433]

[11]. Bishop JA, Nakaguro M, Whaley RD, et al. Oncocytic intraductal carcinoma of salivary glands: a distinct variant with TRIM33-RET fusions and BRAF V600E mutations. Published online November Histopathology 2020. 10.1111/his.14296.

[12]. Skálová A, Vanecek T, Sima R, Laco J, Weinreb I, Perez-Ordonez B, et al. Mammary analogue secretory carcinoma of salivary glands, containing the ETV6-NTRK3 fusion gene: a hitherto undescribed salivary gland tumor entity. Am J Surg Pathol. 2010 May;34: 599–608. 10.1097/PAS.0b013e3181d9efcc. [PubMed: 20410810]

[13]. Griffith C, Seethala R, Chiosea SI. Mammary analogue secretory carcinoma: a new twist to the diagnostic dilemma of zymogen granule poor acinic cell carcinoma. Virchows Arch 2011;459:117–8. 10.1007/s00428-011-1098-6. [PubMed: 21638010]

[14]. Skalova A Mammary analogue secretory carcinoma of salivary gland origin: an update and expanded morphologic and immunohistochemical spectrum of recently described entity. Head Neck Pathol 2013;7:30–6. 10.1007/s12105-013-0455-y.

[15]. Skalova A, Vanecek T, Martinek P, Weinreb I, Stevens TM, Simpson RHW, et al. Molecular profiling of mammary analog secretory carcinoma revealed a subset of tumors harboring a novel ETV6-RET translocation: report of 10 cases. Am J Surg Pathol 2018; 42:234–46. 10.1097/PAS.0000000000000972. [PubMed: 29076873]

[16]. Guilmette J, Dias-Santagata D, Nosé V, Lennerz JK, Sadow PM. Novel gene fusions in secretory carcinoma of the salivary glands: enlarging the ETV6 family. Hum Pathol 2019;83:50–8. 10.1016/j.humpath.2018.08.011. [PubMed: 30130630]

[17]. Amin MB. AJCC Cancer Staging manual. eighth 2017.

[18]. Pfister DG, Spencer S, Adelstein D, Adkins D, Brizel DM. NCCN guidelines version 1.2021, head and neck cancer. https://www.nccn.org/professionals/physician_gls/pdf/head-and-neck.pdf. Accessed 10 Mar 2021.

[19]. Hu B, Jin J, Guo A-Y, Zhang H, Luo J, Gao G. GSDS 2.0: an upgraded gene feature visualization server. Bioinforma Oxf Engl 2015;31:1296–7. 10.1093/bioinformatics/btu817.

[20]. Palicelli A Intraductal carcinomas of the salivary glands: systematic review and classification of 93 published cases. APMIS 2020;128: 191–200. 10.1111/apm.13009. [PubMed: 31697865]

[21]. Rooper LM, Thompson LDR, Gagan J, Oliai BR, Weinreb I, Bishop JA. Salivary intraductal carcinoma arising within intraparotid lymph node: a report of 4 cases with identification of a novel STRN-ALK fusion. Head Neck Pathol 2020. 10.1007/s12105-020-01198-0. Published online July 13.

[22]. Hsieh M-S, Lee Y-H, Jin Y-T, Kuo Y-J. Clinicopathological study of intraductal carcinoma of the salivary gland, with emphasis on the apocrine type. Virchows Arch 2020;477:581–92. 10.1007/s00428-020-02823-7. [PubMed: 32383006]

[23]. Nakaguro M, Urano M, Suzuki H, Yamada K, Sakaguchi A, Ogura K, et al. Low-grade intraductal carcinoma of the salivary gland with prominent oncocytic change: a newly described variant. Histopathology 2018;73:314–20. 10.1111/his.13517. [PubMed: 29574881]

[24]. Wang K, Russell JS, McDermott JD, Elvin JA, Khaira D, Johnson A, et al. Profiling of 149 salivary duct carcinomas, carcinoma ex pleomorphic adenomas, and adenocarcinomas, not

otherwise specified reveals actionable genomic alterations. Clin Canc Res 2016;22: 6061–8. 10.1158/1078-0432.CCR-15-2568.

[25]. McLean-Holden AC, Bishop JA. Low molecular weight cytokeratin immunohistochemistry reveals that most salivary gland Warthin tumors and lymphadenomas arise in intraparotid lymph nodes. Head Neck Pathol 2020. 10.1007/s12105-020-01215-2. Published online August 31.

[26]. Lin S-C, Ko R-T, Kang B-H, Wang J-S. Intraductal carcinoma of salivary gland originating from an intraparotid lymph node: a case report. 2019. p. 5. Published online.

[27]. Bullerdiek J, Wobst G, Meyer-Bolte K, et al. Cytogenetic subtyping of 220 salivary gland pleomorphic adenomas: correlation to occurrence, histological subtype, and in vitro cellular behavior. Canc Genet Cytogenet 1993;65:27–31. 10.1016/0165-4608(93)90054-P.

[28]. Voz ML, ÅstrÖm A-K, Kas K, Mark J, Stenman G, Van de Ven WJ. The recurrent translocation t(5;8)(p13;q12) in pleomorphic adenomas results in upregulation of PLAG1 gene expression under control of the LIFR promoter. Oncogene 1998;16:1409–16. 10.1038/sj.onc.1201660. [PubMed: 9525740]

[29]. Persson F, Andrén Y, Winnes M, Wedell B, Nordkvist A, Gudnadottir G, et al. High-resolution genomic profiling of adenomas and carcinomas of the salivary glands reveals amplification, rearrangement, and fusion of *HMGA2*. Genes Chromosomes Cancer 2009;48:69–82. 10.1002/gcc.20619. [PubMed: 18828159]

[30]. Chiosea SI, Thompson LD, Weinreb I, Bauman JE, Mahaffey AM, Miller C, et al. Subsets of salivary duct carcinoma defined by morphologic evidence of pleomorphic adenoma, *PLAG1* or *HMGA2* rearrangements, and common genetic alterations: classification of Salivary Duct Carcinoma. Cancer 2016;122:3136–44. 10.1002/cncr.30179. [PubMed: 27379604]

[31]. Bahrami A, Dalton JD, Shivakumar B, Krane JF. PLAG1 alteration in carcinoma ex pleomorphic adenoma: immunohistochemical and fluorescence in situ hybridization studies of 22 cases. Head Neck Pathol 2012;6:328–35. 10.1007/s12105-012-0353-8. [PubMed: 22485045]

[32]. de Brito BS, Giovanelli N, Egal ES, Sánchez-Romero C, Nascimento JS, Martins AS, et al. Loss of expression of Plag1 in malignant transformation from pleomorphic adenoma to carcinoma ex pleomorphic adenoma. Hum Pathol 2016;57:152–9. 10.1016/j.humpath.2016.07.011. [PubMed: 27473265]

[33]. Katabi N, Ghossein R, Ho A, Dogan S, Zhang L, Sung YS, et al. Consistent PLAG1 and HMGA2 abnormalities distinguish carcinoma ex-pleomorphic adenoma from its de novo counterparts. Hum Pathol 2015;46:26–33. 10.1016/j.humpath.2014.08.017. [PubMed: 25439740]

[34]. Griffith CC, Thompson LD, Assaad A, Purgina BM, Lai C, Bauman JE, et al. Salivary duct carcinoma and the concept of early carcinoma ex pleomorphic adenoma. Histopathology 2014;65: 854–60. 10.1111/his.12454. [PubMed: 24804831]

[35]. Bishop JA, Rooper LM, Sangoi AR, Gagan J, Thompson LDR, Inagaki H. The myoepithelial cells of salivary intercalated duct-type intraductal carcinoma are neoplastic: a study using combined whole-slide imaging, immunofluorescence, and RET fluorescence in situ hybridization. Am J Surg Pathol 2021;45:507–15. 10.1097/PAS.0000000000001605. [PubMed: 33086236]

[36]. Connor A, Skalova A. Mammary analog secretory carcinoma of salivary gland origin with the ETV6 gene rearrangement by FISH: expanded morphologic and immunohistochemical spectrum of a recently described entity. Am J Surg Pathol 2012;36:8. [PubMed: 22020041]

[37]. Stevens TM, Kovalovsky AO, Velosa C, Shi Q, Dai Q, Owen RP, et al. Mammary analog secretory carcinoma, low-grade salivary duct carcinoma, and mimickers: a comparative study. Mod Pathol 2015; 28:1084–100. 10.1038/modpathol.2015.64. [PubMed: 26089091]

[38]. Shah AA, Wenig BM, LeGallo RD, Mills SE, Stelow EB. Morphology in conjunction with immunohistochemistry is sufficient for the diagnosis of mammary analogue secretory carcinoma. Head Neck Pathol 2015;9:85–95. 10.1007/s12105-014-0557-1. [PubMed: 25078757]

[39]. Sasaki E, Masago K, Fujita S, Suzuki H, Hanai N, Hosoda W. Salivary secretory carcinoma harboring a novel ALK fusion: expanding the molecular characterization of carcinomas beyond the ETV6 gene. Am J Surg Pathol 2020. 10.1097/-PAS.0000000000001471. Publish Ahead of Print.

[40]. Skálová A, Baneckova M, Thompson LDR, Ptáková N, Stevens TM, Brcic L, et al. Expanding the molecular spectrum of secretory carcinoma of salivary glands with a novel VIM-RET fusion. Am J Surg Pathol 2020. 10.1097/PAS.0000000000001535. Publish Ahead of Print.

[41]. Black M, Liu CZ, Onozato M, Iafrate AJ, Darvishian F, Jour G, et al. Concurrent identification of novel EGFR–SEPT14 fusion and ETV6–RET fusion in secretory carcinoma of the salivary gland. Head Neck Pathol 2020;14:817–21. 10.1007/s12105-019-01074-6. [PubMed: 31502214]

[42]. Zhu Z, Ciampi R, Nikiforova MN, Gandhi M, Nikiforov YE. Prevalence of RET/PTC rearrangements in thyroid papillary carcinomas: effects of the detection methods and genetic heterogeneity. J Clin Endocrinol Metab 2006;91:3603–10. 10.1210/jc.2006-1006. [PubMed: 16772343]

[43]. Nikiforov YE. RET/PTC rearrangement–a link between Hashimoto's thyroiditis and thyroid cancer...or not. J Clin Endocrinol Metab 2006;91:2040–2. 10.1210/jc.2006-0791. [PubMed: 16757533]

[44]. Lee SE, Lee B, Hong M, Song JY, Jung K, Lira ME, et al. Comprehensive analysis of RET and ROS1 rearrangement in lung adenocarcinoma. Mod Pathol Off J U S Can Acad Pathol Inc 2015; 28:468–79. 10.1038/modpathol.2014.107.

[45]. Paratala BS, Chung JH, Williams CB, Yilmazel B, Petrosky W, Williams K, et al. RET rearrangements are actionable alterations in breast cancer. Nat Commun 2018;9:4821. 10.1038/s41467-018-07341-4. [PubMed: 30446652]

[46]. Amit M, Na'ara S, Leider-Trejo L, Binenbaum Y, Kulish N, Fridman E, et al. Upregulation of RET induces perineurial invasion of pancreatic adenocarcinoma. Oncogene 2017;36:3232–9. 10.1038/onc.2016.483. [PubMed: 28092668]

[47]. Zhao Z, Fu T, Gao J, Xu Y, Wu X, Chen W, et al. Identifying novel oncogenic RET mutations and characterising their sensitivity to RET-specific inhibitors. J Med Genet 2020. 10.1136/jmedgenet-2019-106546. Published online April.

[48]. Kato S, Subbiah V, Marchlik E, Elkin SK, Carter JL, Kurzrock R. RET aberrations in diverse cancers: next-generation sequencing of 4,871 patients. Clin Cancer Res Off J Am Assoc Cancer Res 2017;23: 1988–97. 10.1158/1078-0432.CCR-16-1679.

[49]. Petursson SR. Metastatic medullary thyroid carcinoma: complete response to combination chemotherapy with dacarbazine and 5-fluorouracil. Cancer 1988;62:1899–903. 10.1002/1097-0142(19881101)62:9<1899::AID-CNCR2820620905>3.0.CO;2-C. [PubMed: 3167804]

[50]. Elisei R, Schlumberger MJ, Müller SP, Schöffski P, Brose MS, Shah MH, et al. Cabozantinib in progressive medullary thyroid cancer. J Clin Oncol 2013;31:3639–46. 10.1200/JCO.2012.48.4659. [PubMed: 24002501]

[51]. Wells SA Jr, Robinson BG, Gagel RF, Dralle H, Fagin JA, Santoro M, et al. Vandetanib in patients with locally advanced or metastatic medullary thyroid cancer: a randomized, double-blind phase III trial. J Clin Oncol 2012;30:134–41. 10.1200/JCO.2011.35.5040. [PubMed: 22025146]

[52]. Wirth L, Sherman E, Drilon A, Solomon B, Robinson B, Lorch J, et al. Registrational results of LOXO-292 in patients with RET-altered thyroid cancers. Ann Oncol 2019;30:v933. 10.1093/annonc/mdz394.093.

[53]. Subbiah V, Gainor JF, Rahal R, Brubaker JD, Kim JL, Maynard M, et al. Precision targeted therapy with BLU-667 for RET-driven cancers. Canc Discov 2018;8:836–49. 10.1158/2159-8290.CD-18-0338.

[54]. Wirth LJ, Sherman E, Robinson B, Solomon B, Kang H, Lorch J, et al. Efficacy of selpercatinib in *RET*-altered thyroid cancers. N Engl J Med 2020;383:825–35. 10.1056/NEJMoa2005651. [PubMed: 32846061]

[55]. Subbiah V, Cote GJ. Advances in targeting RET-dependent cancers. Canc Discov 2020;10:498–505. 10.1158/2159-8290.CD-19-1116.

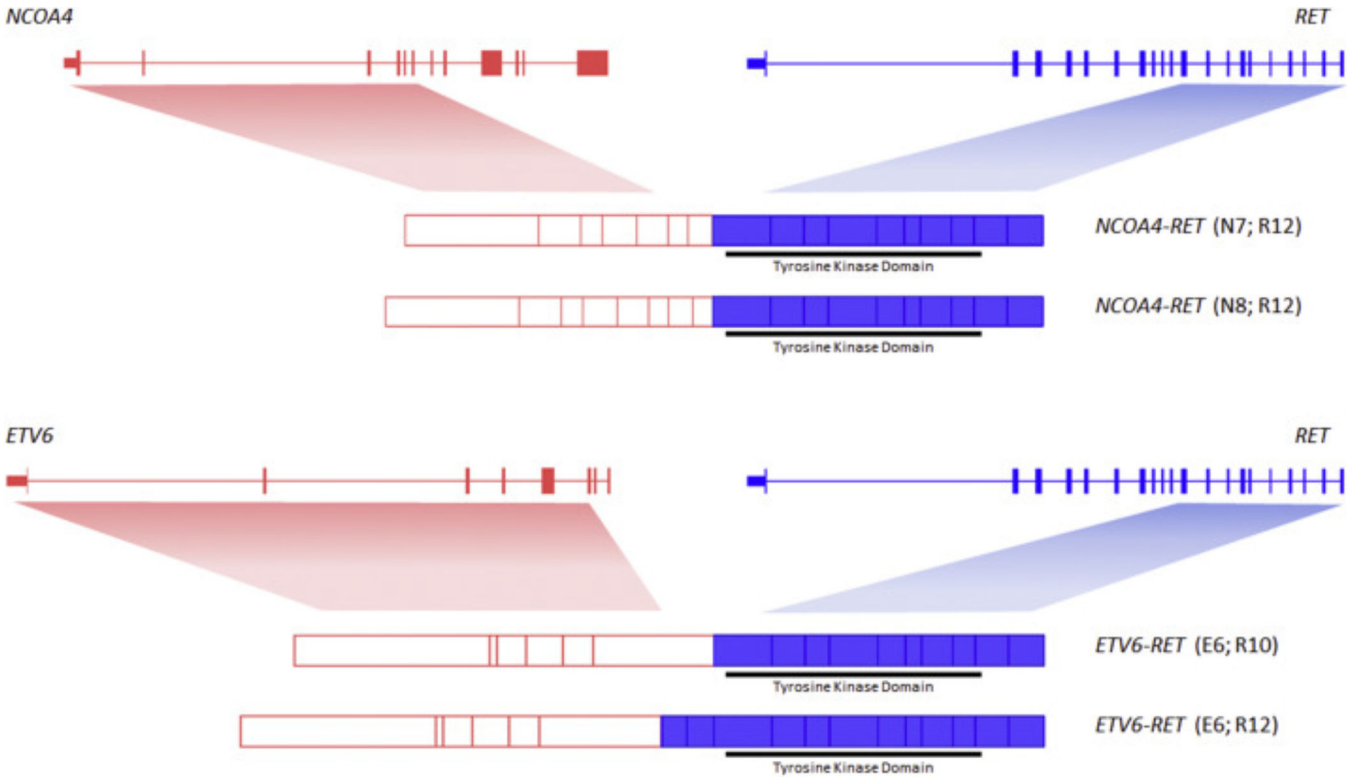

Fig. 1.

Schematic representation of *RET* gene rearrangements identified in salivary carcinoma. (A) *NCOA4-RET* isoforms include the fusion of exon 7 or exon 8 of *NCOA4* (red) with exon 12 of RET (blue); (B) *ETV6-RET* isoforms include the fusion of exon 6 of *ETV6* (red) with exon 10 or exon 12 of *RET* (blue). In the diagrams, the intron/exon structure of each fusion partner is depicted on the top panel, and the corresponding fusion transcripts are illustrated at the bottom. The images were generated using the Gene Structure Display Server 2.0 (http://gsds.cbi.pku.edu.cn) [18] and the following transcript identifiers: *ETV6* (ENST00000396373.4), *NCOA4* (ENST00000452682.1), and *RET* (ENST00000355710.3), obtained from the Ensembl GRCh37 release 100—April 2020 (http://grch37.ensembl.org/). The exons are displayed at the same scale for the three genes. To facilitate visualization, intron sizes were reduced to one-tenth of their original size for *ETV6* and to half of their original size for *NCOA4* and *RET*.

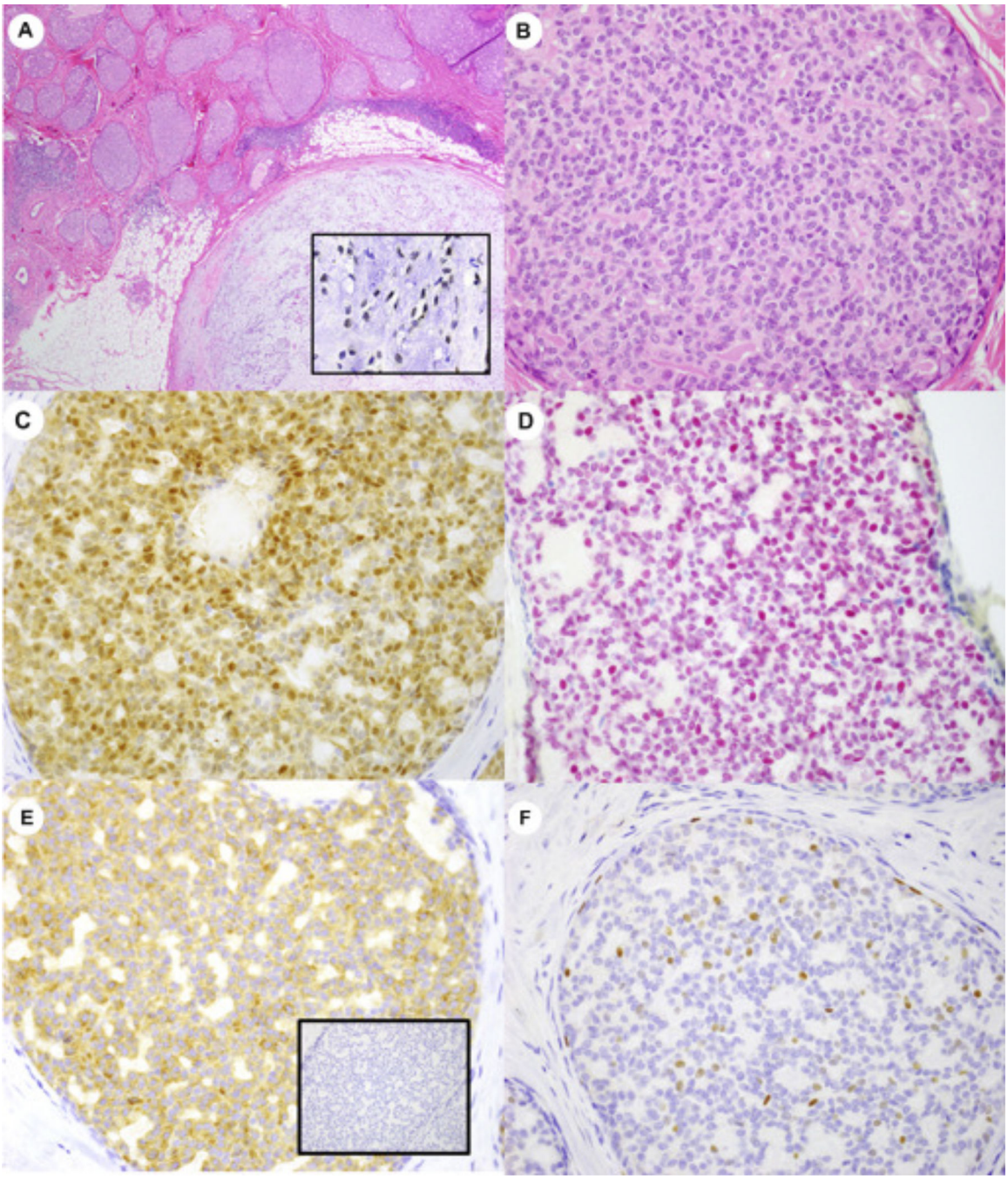

Fig. 2.

Case 5, intercalated duct intraductal carcinoma arising in contiguity with a pleomorphic adenoma (A; 40×) with nuclear reactivity for PLAG1 by immunohistochemistry (A inset, 1000×) in the pleomorphic adenoma only, and typical morphological features including low-grade nuclei, eosinophilic cytoplasm, and circumscription by myoepithelial cells in the intraductal carcinoma (B; 400×). Tumor cells are positive by immunohistochemistry for S100 (C), SOX10 (D), and mammaglobin (E), and are negative for androgen receptor (E inset). Myoepithelial cells and rare tumor cells are highlighted by p63 (F).

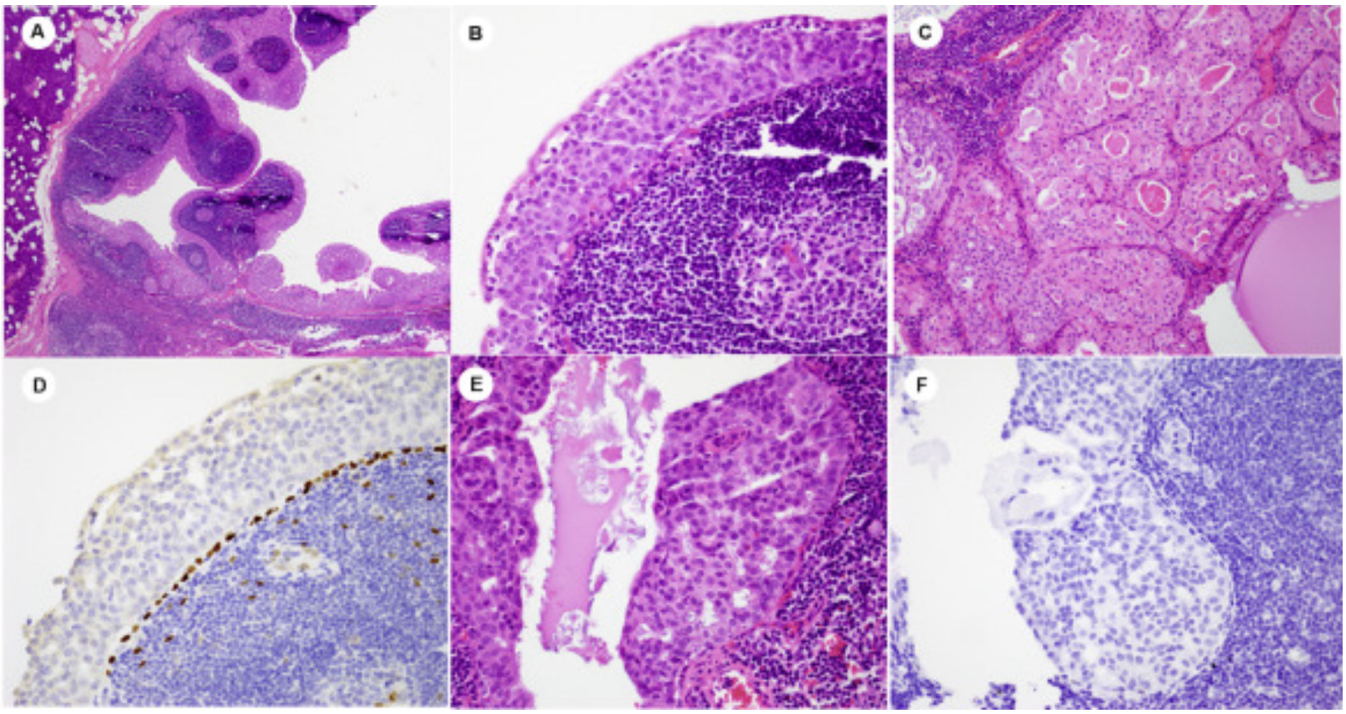

Fig. 3.

Case 2, intraductal carcinoma arising in an intraparotid lymph node (A; 20×), with intercalated duct morphology (3B; 400×) and a focal oncocytic component (C). The majority of the tumor has a preserved myoepithelial lining (3), except for one tumor nodule showing broad invasion (E), evidenced by loss of p63 on immunohistochemistry (F).

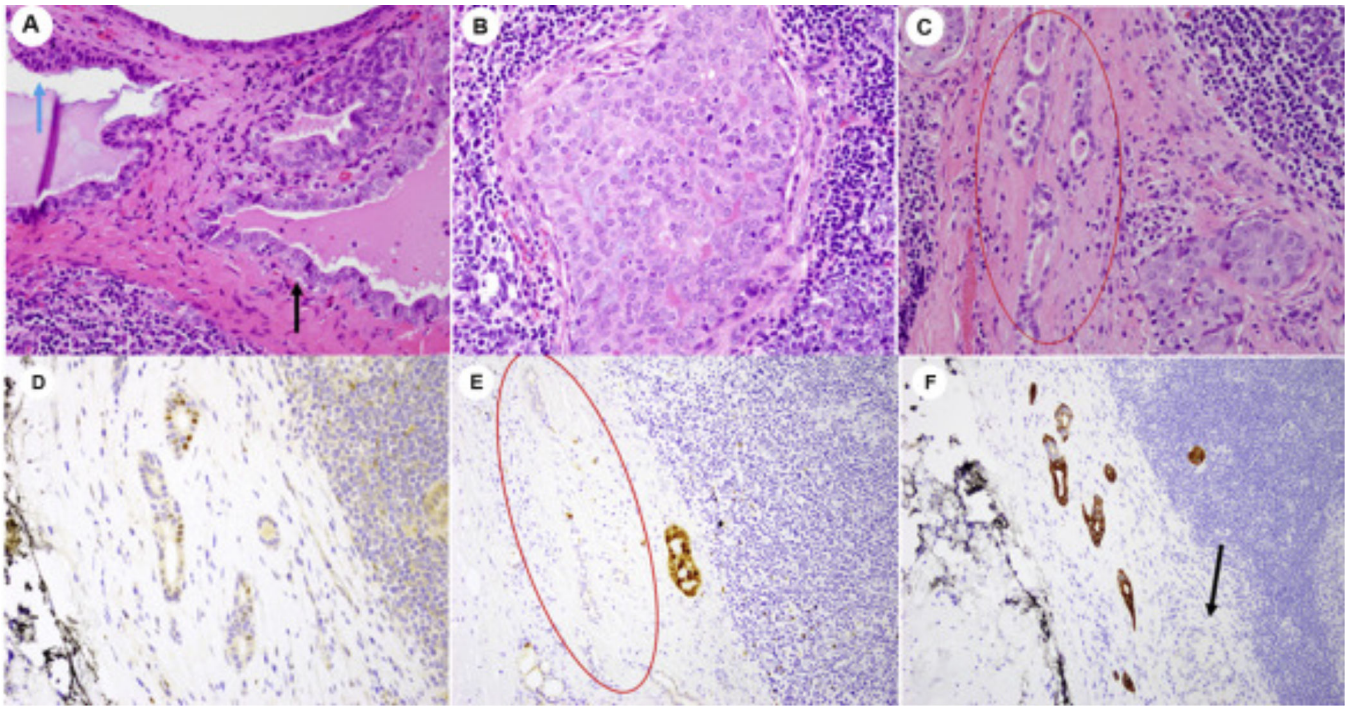

Fig. 4.

Case 4, hybrid intraductal carcinoma with low (blue arrow) to intermediate (black arrow) grade cytologic atypia in the intercalated duct component (4A; 400×), as well as mucinous change in the intermediate-grade areas (4), confirmed by mucicarmine (not shown). The apocrine component is focal (C; 400×) but best visualized on immunohistochemistry, with nuclear reactivity for androgen receptor (D) and S100 loss (E), with intercalated duct nodule for comparison. CK5/6 highlights the intact myoepithelial layer around the minute apocrine glands (F) and is noticeably absent in a nearby focus of invasive intercalated duct component (arrow). Red circle: apocrine component.

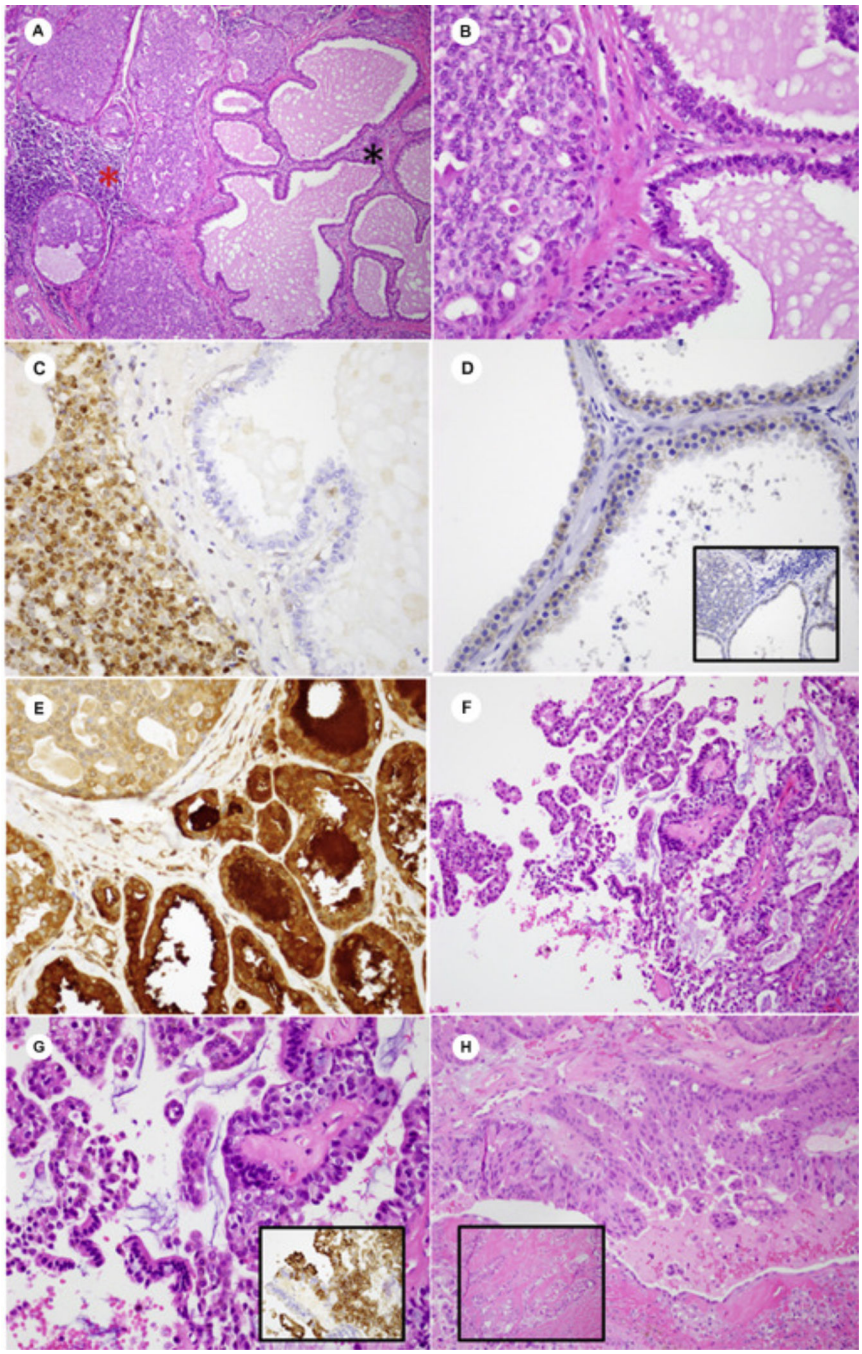

Fig. 5.

Case 6, hybrid intraductal carcinoma (A; 100×) with intercalated duct (red asterisk) and apocrine components (black asterisk). High-power examination shows intercalated duct component with cribriform architecture on the left and classic apocrine morphology on the right, including tumor cells containing abundant eosinophilic cytoplasm apical snouts and luminal decapitations (B; 400×). Immunohistochemistry demonstrates S100 (C) staining in the intercalated duct component and loss in the apocrine component, whereas HER2 was relatively increased in the apocrine component (D), showing stronger and more

diffuse staining than in the intercalated duct component (D inset). Mammaglobin showed diffuse staining in both components (E). A large papillary proliferation (F; 200×) showed heterogeneous morphology (G; 400×) and immunophenotype, as demonstrated by S100 (G inset). In comparison, pure apocrine intraductal carcinomas (5; 400×) show higher grade cytomorphology and features of overt malignancy, including invasion (5 inset).

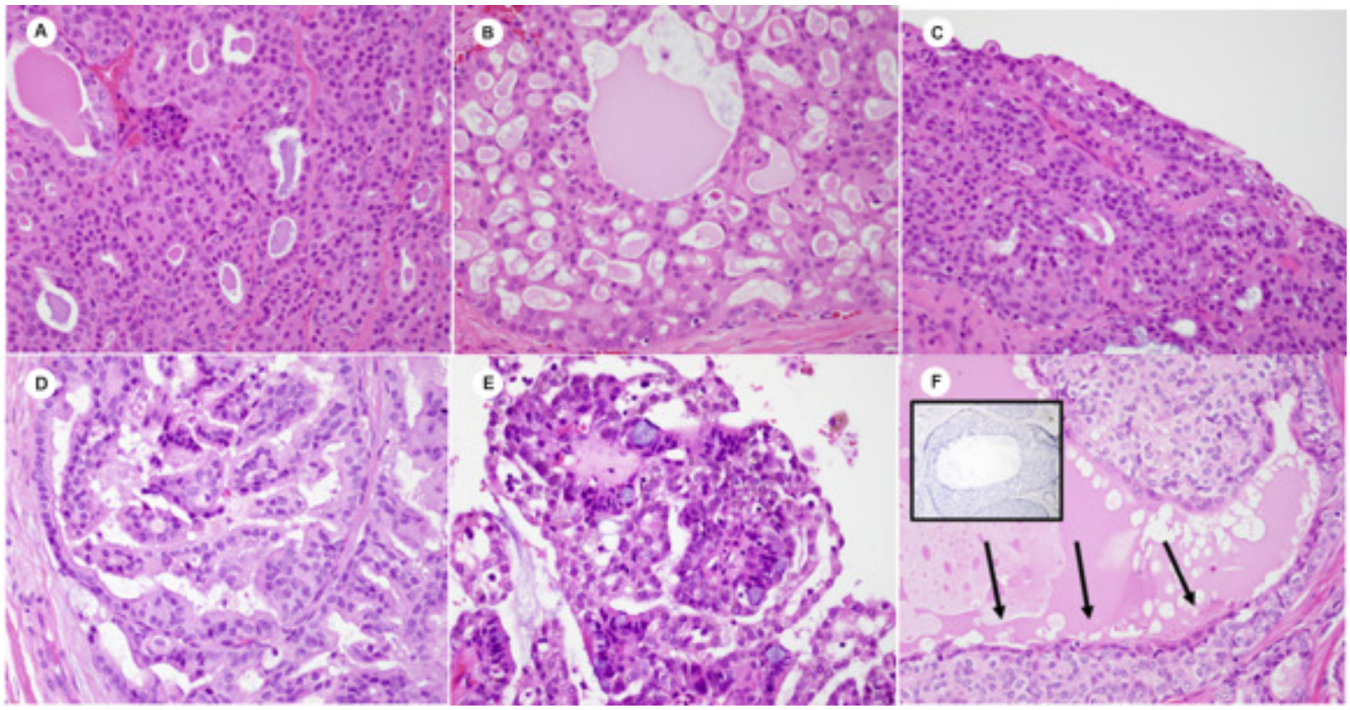

Fig. 6.

Histological comparison of *RET*-translocated salivary gland carcinomas, including intraductal carcinoma (A; 400×) and secretory carcinoma (B; 400×), with both neoplasms showing mildly atypical round-to-ovoid nuclei, eosinophilic cytoplasm, and cribriform spaces containing eosinophilic secretions. Cytoplasmic vacuolation is seen in intercalated duct intraductal carcinoma (C) as well as *RET*-translocated secretory carcinoma (D). In intraductal carcinoma, vacuolated cells are often found at the luminal border of cystic spaces (E and F), where there is often mucinous metaplasia (F) and a layer of elongated, perpendicularly oriented “umbrella”-like cells with abundant, intensely staining eosinophilic cytoplasm (F, arrows). These cells do not stain with myoepithelial markers, such as p63 (F inset).

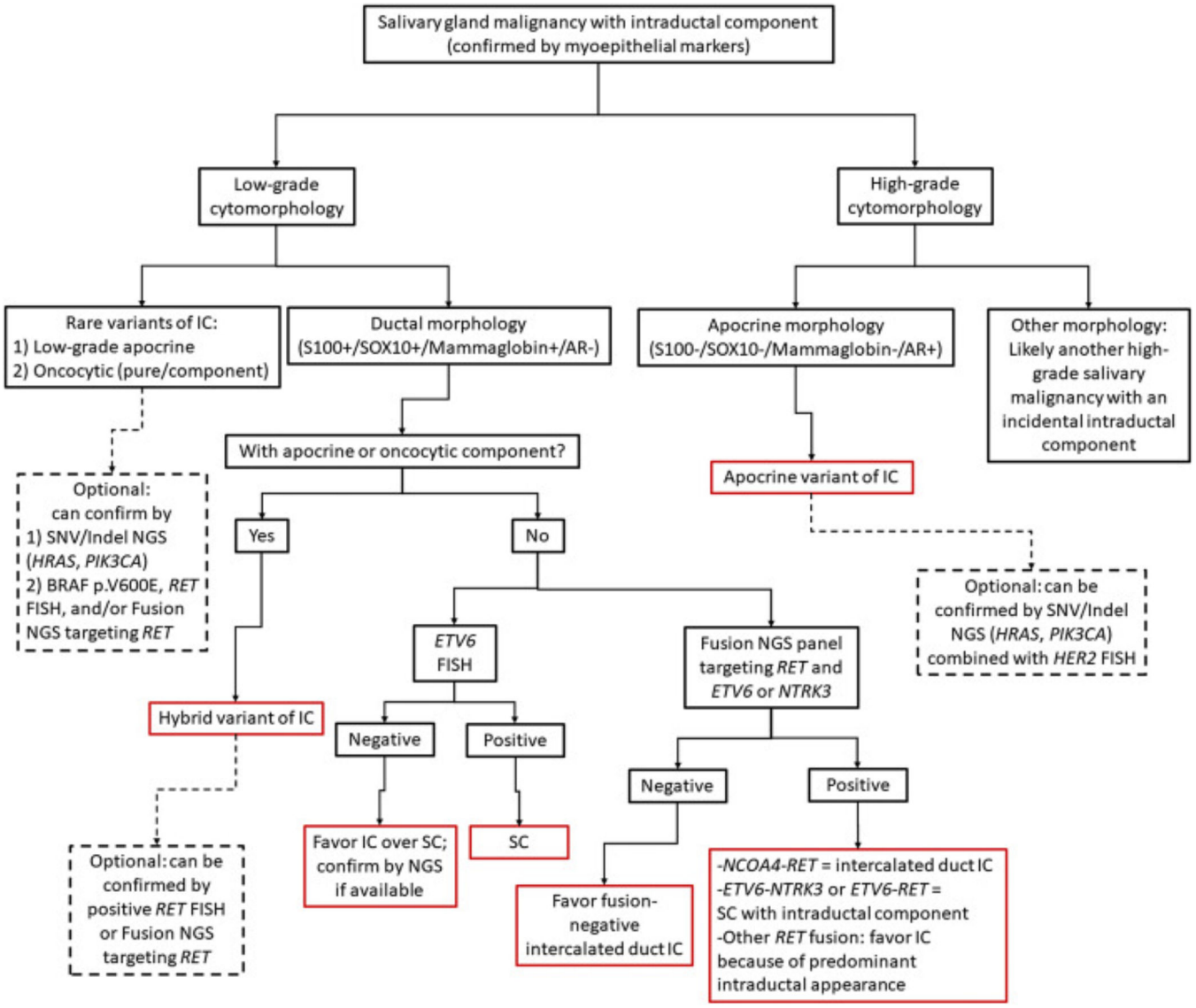

Fig. 7.

Diagnostic flowchart for salivary gland malignancies with entirely or predominantly intraductal component. Instances where a diagnosis is favored over another is based on the preponderance of reported cases with the given feature, for example, molecular alteration. In advanced disease, a specific molecular driver must be identified for targeted therapy. Molecular alterations listed for rare variants of IC are listed in order of the respective variants. Confirmation of hybrid variant by *RET* FISH will be more easily appreciated with *TRIM27*-RET fusions than *NCOA4-RET* fusions, as the latter are intrachromosomal. FISH, fluorescence in situ hybridization; IC, intraductal carcinoma; Indel, insertion-deletion; NGS, next-generation sequencing; SC, secretory carcinoma; SNV, single-nucleotide variant. Red lines indicate diagnostic result. Dashed lines indicate supportive testing that is not necessary for confirmation.

Table 1

Clinicopathologic features and clinical outcomes of intraductal and secretory carcinomas in this study.

Case	Age/ sex	Site, size (cm)	NGS results (fusion exons)	Histomorphology	Margin	Tumor extension			Immunohistochemical profile				Symptoms (duration in months)	TNM[a]/ prognostic stage	Treatment	Follow-up (months), outcome
						LVI	PNI	EGE	Mammaglobin	S100	SOX10	AR				
1	69/F	Parotid, 2.0	*NCOA4-RET (7–12)*	Intercalated duct IC, focally oncocytic, cystic growth, sclerotic stroma with minor component of TALP	Close	(−)	(−)	(−)	(+)	(+)	(+)	Negative	Painless mass (6)	T1Nx/ Stage I	Resection	11, NED
2	61/ M	Parotid, 3.0	*NCOA4-RET (6–12)*	Intercalated duct IC, focally oncocytic, broadly invasive, cystic growth, intraparotid lymph node	Close	(−)	(−)	(−)	(+)	(+)	(+)	Negative	Painless mass (2)	T2Nx/ Stage II	Resection	7, NED
3	88/F	Parotid, 2.2[b]	*NCOA4-RET (6–12)*	Intercalated duct IC, minimally invasive, nodular, stroma with TALP	NA	(−)	(−)[c]	NA[d]	(+)	(+)	(+)	Negative	Painless mass (>48)	cT2N0M0/ Stage II	XRT	25, NED
4	44/F	Parotid, 1.4	*NCOA4-RET (7–12)*	Hybrid IC (intercalated duct predominant), minimally invasive, nodular, sclerotic stroma with TALP, intermediate morphology	Positive	(−)	(−)	(−)	(+)[e]	(+)[e]	(+)[e]	(+)[f]	Painless mass (12)	T1Nx/ Stage I	Resection	63, NED
5	47/F	Parotid, 2.0	*NCOA4-RET (6–12)*	Intercalated duct IC, nodular, sclerotic stroma, diagnosed abutting pleomorphic adenoma	Negative	(+)	(+)[c]	(+)	(+)	(+)	(+)	Negative	Painless mass (22)	T1N0/ Stage I	Resection, XRT	23, NED
6	55/ M	Parotid, 2.5	*NCOA4-RET (6–12)*	Hybrid IC, nodular, sclerotic stroma with TALP	Positive	(−)	(−)	(−)	(+)[e]	(+)[e]	(+)[e]	Negative	Painless mass (1)	T2Nx/ Stage II	Resection, XRT	4, NED
7	61/F	Parotid, 3.8	*HRAS p.Q16K, PIK3CA p.E542K*	Apocrine IC, broadly invasive, cystic, nodular, and infiltrative, sclerotic stroma,	Close	(−)	(−)	(−)	(+)	(−)	(−)	Positive	Painful mass (24)	T2N0/ Stage II	Resection	<1, NED

Case	Age/ sex	Site, size (cm)	NGS results (fusion exons)	Histomorphology	Margin	Tumor extension			Immunohistochemical profile				Symptoms (duration in months)	TNM[a]/ prognostic stage	Treatment	Follow-up (months), outcome
						LVI	PNI	EGE	Mammaglobin	S100	SOX10	AR				
				intermediate- to high-grade morphology												
8	42/ M	Parotid, 2.9	*ETV6-RET (6–12)*	SC, broadly invasive, nodular, sclerotic stroma	Close	(+)	(−)	(+)	(+)	(+)	(+)	Negative	Painless mass (<1)	T2N0/ Stage II	Resection, NND, XRT	78, NED
9	47/ M	Submandibular, NA	*ETV6-RET (6–12)*[g]	SC, broadly invasive, nodular, sclerotic stroma, low-grade to intermediate-grade morphology	NA	NA	NA	NA	(+)	(+)	(+)	Negative	NA	NA	Resection, XRT	300, TR at 252 and 276, NED × 24
10	45/F	Parotid, 1.5	*ETV6-RET (6–12)*	SC, broadly invasive, nodular, sclerotic stroma, low-grade to intermediate-grade morphology	NA	(−)	(−)	(+)	(−)/Rare	(+)	(+)	NA	NA	NA	Resection, NND, XRT	337, TR at 283 and 314, NED × 21
11	53/F	Parotid, 3.0	*ETV6-RET (6–12)*[g]	SC (NA)	NA	NA	NA	NA	(+)	(+)	NA	Negative	NA	cStage IVC	Chemotherapy, alectinib	3, DOD

Cases 3, 5,8, 9, and 11 were published in a study by Guilmette et al. [16].

Immunohistochemical findings in Cases 9 and 10 are from recurrent tumor, and in Case 11 is by report.

Abbreviations: AR, androgen receptor; Bx, not evaluated on biopsy; c, clinically staged; DOD, died of disease; EGE, extraglandular extension; IC, intraductal carcinoma; LVI, lymphovascular invasion; NA, not available for evaluation; NED, alive with no evidence of disease; NND, neck lymph nodes dissection; PNI, perineural invasion; SC, secretory carcinoma; TALP, tumor-associated lymphoid proliferation; TR, tumor recurrence; XTR, external radiation therapy.

[a] Pathologic stage.

[b] Tumor size was reported based on the imaging report.

[c] Tumor involving facial nerve intraoperatively.

[d] Could not be evaluated on biopsy.

[e] Positive reactivity in intercalated duct component.

[f] Positive reactivity in apocrine component.

[g] RET rearrangement confirmed by FISH.